Transitions of water-drop impact behaviour on hydrophobic and hydrophilic particles

C. A. E. HAMLETT[a], S. ATHERTON[a], N. J. SHIRTCLIFFE[b], G. MCHALE[a,d], S. AHN[c], S. H. DOERR[c], R. BRYANT[c] and M. I. NEWTON[a]

[a]School of Science and Technology, Nottingham Trent University, Clifton Lane, Nottingham, NG11 8NS, United Kingdom,

[b]Technology and Bionics, Hochschule Rhine-Waal, Landwehr 4, 47533 Kleve, Germany,

[c]College of Science, Swansea University, Singleton Park, Swansea, SA2 8PP, United Kingdom, [d]Now at School of Computing, Engineering and Information Sciences, Northumbria University, Newcastle upon Tyne, NE1 8ST, United Kingdom

Correspondence: Christopher A.E. Hamlett. E-mail: christopher.hamlett@ntu.ac.uk, alternative: glen.mchale@northumbria.ac.uk

Summary

Extreme soil water repellency can have substantial implications for soil hydrology, plant growth and erosion, including enhanced splash erosion caused by raindrop impact. Previous studies of water droplet impact behaviour on man-made super-hydrophobic surfaces, with which water-repellent soil shares similar characteristics, revealed three distinct modes of splash behaviour (rebound, pinning and fragmentation) distinguished by two transition velocities: rebound-to-pinning (v_{min}) and pinning-to-fragmentation (v*). By using high-speed videography of single water droplet impacts we show that splash behaviour is influenced by the hydrophobicity of immobile particles, with hydrophobic glass spheres exhibiting all three modes of splash behaviour in the hydrophobic state but hydrophilic spheres exhibiting solely pinning behaviour. We found that increasing the particle size of fixed glass spheres increases vmin. A study of droplet impact on hydrophobic sand shows that the increased roughness of the immobile particles makes impacting droplets more likely to fragment at slower impact velocities. The mobility of the particles influenced droplet impact behaviour, with loose, hydrophobic particles displaying significantly greater v_{min} values than their fixed analogues. The surface tension of the water droplet also lifted loose, hydrophobic particles from the surface, forming highly mobile 'liquid marbles'. Water-repellent soil was also shown to form 'liquid marbles' at both the slow (approximately 0.3–2.1 m s^{-1}) and fast (about 7 m s^{-1}) droplet impact velocities studied. The observation of very mobile liquid marbles upon water droplet impact on water-repellent soil is significant as this provided a mechanism that may enhance erosion rates of water-repellent soil.

Introduction

Water-repellent behaviour is a common feature of many soils under a wide range of land uses, and occurs in susceptible soils when their water content is less than a soil-specific threshold (Dekker et al., 2001; Doerr et al., 2006). The primary implications of this behaviour from a soil physics perspective include: (i) reduced infiltration rates and a corresponding increase in the likelihood and amount of infiltration-excess (Hortonian) overland flow; (ii) more spatial variability in infiltration and soil moisture retention, causing an uneven distribution of soil moisture; (iii) enhanced surface erosion aided by the increase in overland flow and (iv) greater susceptibility to wind erosion caused by drier soil conditions and reduced cohesion of soil particles (DeBano, 2000; Doerr et al., 2000). Such reduced infiltration can also have secondary effects, such as hindering the germination and growth of vegetation (DeBano, 2000; Doerr et al., 2000; Hallett et al., 2004). A range of approaches to ameliorate more extreme forms of water repellency has been developed (Mueller & Deurer, 2011). Soil is classed as extremely water repellent when water droplets placed on the soil surface do not infiltrate within 1 hour (water drop penetration time (WDPT) test (Bisdom et al., 1993)) or a solution with an ethanol concentration of > 24% is required to allow droplet penetration within 3 s (Molarity of an Ethanol Droplet (MED) or %ethanol test (Dekker & Ritsema, 1994; Doerr et al., 1998)). MED tests have also been used to show that the particle size and arrangement of close packed, hydrophobic glass spheres influence the penetration of liquid into the bead bed (Hamlett et al., 2011).

Most common soil minerals are naturally hydrophilic and the presence of organic compounds with hydrophobic properties is required to render a mineral particle surface water repellent (Doerr et al., 2000; Ellerbrock et al., 2005; Atanassova & Doerr, 2010). The interplay between the intrinsic water repellency of the surface chemistry of the water repellent soil particles and their complex, rough topography (both of the soil matrix and of the individual particles) that is believed to induce extreme water repellency (McHale et al., 2005; Shirtcliffe et al., 2006; McHale et al., 2007; Bachmann & McHale, 2009) and is believed to play a key role in enhanced soil erosion when rainfall occurs (Terry & Shakesby, 1993). By displaying a combination of intrinsic chemical hydrophobicity and a rough topography water repellent soil lends itself to comparisons with superhydrophboic surfaces (Roach et al., 2008) and previous studies of water droplet impact on such surfaces (Reysatt et al., 2006; Tsai et al., 2009) have identified three regimes of velocity-dependant droplet behaviour, which are rebound, pinning and fragmentation. The transition velocities between the different droplet impact behaviour regimes occur at low impact velocities (< ~ 2 $m.s^{-1}$) compared to that of rainfall (9 - 13 $m.s^{-1}$) (Beard, 1976). Although a similar effect has been argued to occur to granular, porous hydrophobic materials like some soils, a direct observation of the phenomenon has yet to be conducted.

This study presents a step-wise investigation linking studies on 'ideal' (super)-hydrophobic surfaces (Reyssat et al., 2006; Tsai et al., 2009; Lee & Lee, 2011) to water-repellent soil. Our approach is to compare the impact behaviour of individual water droplets on granular systems at impact velocities similar to those previously studied on super-hydrophobic surfaces (< about 2 m s^{-1}) and extend this to faster impact velocities about 7 m s^{-1}) which are much closer to the slower terminal velocities of raindrops. The influence of the intrinsic chemical hydrophobicity of fixed glass spheres on

single water droplet impact behaviour is presented along with the effect of particle size of fixed, hydrophobic glass spheres on the droplet impact transitions. This study is then extended to examine differences of the transition velocities between fixed and loose glass spheres. Subsequently, the droplet impact behaviour on treated sand was studied to investigate the influence of the effect of particle shape on the transition velocities.

The aims of this study were to (i) investigate the various factors that influence the behaviour of water droplets upon impact on water-repellent and wettable particulate matter and (ii) to explore whether glass particles can provide a realistic model for naturally occurring highly water-repellent soil.

Materials and methods

This study involved preparing hydrophilic and hydrophobic samples of both glass spheres and sand. The samples were then prepared for testing by either immobilizing a single layer of particles on glass microscope slides (fixed samples) or by pouring the particles into a holder (loose samples). The impact behavior of single water droplets on the samples were investigated using high speed videography. Prior to the droplet impact experiments the effect on water repellency of the surface treatments were determined either by contact angle analysis, on fixed, single layers of particles or on flat microscope slides, or by MED tests on loose, multilayered particle samples. The methods used to measure water repellency will be described first.

Determination of the degree of water repellency

Contact angle analysis was carried out on hydrophobic and hydrophilic glass microscope slides and on fixed hydrophobic glass spheres using a Krüss DSA 10 contact angle meter and analysed using Krüss DSA software. The (observed) static contact angle (θ) was measured by placing a water droplet (15 µl) on a surface. The volume of the droplet was then increased and decreased to measure the advancing (θ_A) and receding (θ_R) contact angles, which are the contact angles at which the solid-liquid-vapour interface point just begins to advance and recede respectively. We note that these observed contact angles differ from the Young's law contact angle, which is often referred to in the wetting literature. This intrinsic contact angle is defined from a combination of the solid-liquid, solid-vapour and liquid-vapour interfacial tensions and represents the surface chemistry of the solid (with or without surface treatment) of an individual particle (see, e.g., McHale & Newton, 2011).

The MED or % ethanol test (Dekker & Ritsema, 1994; Doerr et al., 1998) was used to determine the severity of water repellency for the samples consisting of loose particles. The test involved determining the ethanol concentration required in droplets placed on the sample surface to penetrate within 3 s. Concentrations used were 0 and 3 % (wettable), 5% (slightly-), 8.5% (moderately-), 13% (strongly-), 24% (very strongly-) and 36% (extremely water repellent) (Doerr et al., 1998). The test was carried out on 5 subsamples each, with each test for the beads, sand and soil samples falling into the same respective %ethanol category (see Tables S1-4 for results of MED/ % ethanol tests). The MED/ % ethanol test was not an appropriate for water repellency severity of single layers of fixed glass

spheres as the single layer had insufficient depth to allow drop penetration. Therefore, the contact angle method was used to clarify the hydrophobicity of the surface treatments carried out on the particles used to make single layered samples.

Preparation of glass spheres

Spherical glass spheres (General purpose glass microspheres, Whitehouse Scientific) of various sieve fractions in the range 32 – 212 μm range (sieve sizes: 32-45, 63-75, 75-80, 80-90, 90-106, 125-140 and 180-212 μm) were passed through sieves (stainless steel wire mesh test sieves - Endecotts) of various aperture sizes (50, 75, 80, 90, 106, 112, 125, 150, 180, 212 and 250 μm) to obtain the sieve fractions listed in Table 1. The particles were then immersed in 30 vol% hydrochloric acid (HCl) (diluted from 36% HCl, Fisher Scientific, UK) for 24 hrs, rinsed with copious amounts of water (resistivity = 18 $M\Omega.cm^{-1}$, which was used throughout), dried for 4 hrs at 110 °C and allowed to cool to room temperature.

	Contact angle / °			v_{min} / m s^{-1}	
Particle size / μm	Static	Advancing	Receding	3-μl droplet	6-μl droplet
32–45	112 ± 16	128 ± 14	68 ± 12	0.4	0.4
63–75	126 ± 5	134 ± 7	93 ± 29	0.5	0.6
75–80	136 ± 2	141 ± 4	128 ± 4	0.6	0.5
80–90	135 ± 4	142 ± 3	128 ± 7	0.6	0.6
90–106	128 ± 3	137 ± 3	102 ± 9	0.6	0.5
125–140	134 ± 2	141 ± 3	124 ± 4	0.7	0.7
180–212	127 ± 4	138 ± 7	112 ± 11	0.8	0.7

The contact angle data shown are the average of seven measurements, and standard deviation is shown.

Table 1. Contact angle data of fixed layers of hydrophobic particles. The contact angle data shown is the average of seven measurements, standard deviation is shown as the error.

In order to render samples hydrophobic and loose, they were then immersed in 'Extreme Wash In' solution (Grangers, Alfreton, UK) (5 % v/v solution in water) for 30 minutes and then dried at 80◦ C for 4 hours.

Preparation of sand and soil samples

Natural sand, taken from fluvial deposits in Swansea Bay (51° 36' 19"N, 3° 58' 58" W) was sieved to obtain the 180–212μm sieve fraction to allow later comparisons with glass beads of the same sieve fraction. The sand was then immersed in HCl (3% v/v in water) for 16 hours, then rinsed with copious

amounts of water and immersed in HCl (3 % v/v in water). After 3 hours, the concentration of HCl was gradually increased to 30 % v/v in water and the sand was left in the HCl for 1 hour at room temperature. The sand was then rinsed with water (3×100 ml), 5 m KOH solution (3×100 ml) and water (3×100 ml) and immersed in HCl (30 % v/v in water) for 16 hours, then rinsed with water (5×50 ml) and dried for 3 hours at 80◦ C.

The sand was rendered hydrophobic by immersion in 'Extreme Wash In' solution (Grangers) (5 % v/v solution in water) for 30 minutes and then dried at 80◦ C for 4 hours. The sand was extremely water repellent according to the MED/% ethanol test described earlier. A 36% ethanol solution did not penetrate the sample within 3 s. This material was used as a simple model analogue for a sandy water-repellent soil with a narrow particle size distribution. In addition, naturally water repellent surface soil material (Humic Cambisol of sandy loam texture), was taken at 0-5 cm depth from a dense Eucalyptus globulus plantation over granitic bedrock in northern Portugal (41°26'06'' N, 8°15'34'' W). This soil sample was air dried, but otherwise untreated, to provide a naturally water repellent soil material in drop impact experiments. It was very strongly water repellent, requiring a 24% ethanol solution for drop penetration (see % ethanol test below). Soil solution pH was 5.4, as determined with a Hanna portable pH meter using 5 g soil in 25 ml of distilled water.

In addition, naturally water-repellent surface soil material Humic Cambisol of sandy loam texture) was taken at 0–5 cm depth from a dense Eucalyptus globulus Labill. plantation over granitic bedrock in northern Portugal (41^{o} 26' 06" N, 8^{o} 15' 34" W). This soil sample was air-dried, but otherwise untreated, to provide naturally water-repellent soil material. It was very strongly water repellent, requiring a 24% ethanol solution for drop penetration see % ethanol test later). Soil solution pH was 5.4, as determined with a portable pH meter (Hanna, Leighton Buzzard, UK) with 5 g soil in 25 ml of distilled water.

Preparation of particulate samples for impact testing

To prepare layers of fixed particles loose, hydrophilic particles (either glass spheres or sand particles) were first placed in a petri dish and then a glass microscope slide, which had been coated with a thin (~ 20 μm thick), tacky layer of polyurethane adhesive (1A33, Humiseal), was pressed into the top of the loose bed of particles. The microscope slide was then removed, having lifted a layer of particles from the loose bed, and cured at 80 °C for 16 hrs to set the adhesive during which time the adhesive does not migrate from the microscope slide and up the sides of the glass spheres. At this stage the samples are ready to be used as fixed, hydrophilic particles. For the preparation of fixed, hydrophobic samples, the particle loaded glass microscope slides were then immersed in 'Extreme Wash In' solution (Grangers) (5 vol% in water) for 30 mins and then dried at 80 °C for 4 hrs.

Loose particulate samples were prepared by cutting out equilateral triangular frames (with length of side of 15 mm) from 440 μm thick acetate sheet, which were then glued to a glass microscope slide using polyurethane adhesive (1A33, Humiseal). Two further acetate frames were glues on top of

the base frame with polyurethane adhesive (1A33, Humiseal) and then cured at 80 °C for 16 hrs. The loose particles were then poured into the frame and tapped down by resting a microscope slide on top of them; this was then removed prior to the droplet impact experiments.

Drop impact experiments

For slow impact velocity experiments (v≤about 2.1 m s^{-1}) the sample and syringe needle were enclosed in an acrylic box in order to minimize air flow (Figure S1). The needle was attached to a water-filled syringe, located outside of the box, by plastic tubing and mounted between two clamp stands. The clamp stands were marked to indicate the needle tip-to-sample distance in order to facilitate measurement of the transitional droplet heights (h_{min} and h*) corresponding with drop impact behaviour (the rebound to-pinning and pinning-to-fragmentation transitions, respectively, as described in Results and Discussion). The needle tip-to sample heights were converted into transition velocities using the equations of a calibration curve (Figure S2).

In order to control the size of the droplet, separate flat ended syringe needles of two different gauges were used to deliver droplets of two different droplet volumes, with 20G and 26G needles used to dispense droplets with volumes of about 6 and 3 µl, respectively. Fourteen recordings were made of each combination of drop height and particle size and for at least two droplet heights of 0.5-cm increments either side of the relevant transition height. The maximum drop height possible in this system was 30 cm, which was high enough to provide sufficient impact velocity to observe fragmentation, thus both transition velocities, for all samples studied. However, the impact velocities studied with such a system (v ≤ about 2.1 m s^{-1}) are far slower than those of a raindrop impacting soil at terminal velocity (9–13 m s^{-1}) (Beard, 1976), but may be comparable to impacts of drops reaching the ground from some irrigation systems or following interception by vegetation.

For the greater velocity droplet impact experiments droplet heights of ~3.5 m were used and these achieved typical impact velocities of ~7 $m.s^{-1}$. For such experiments a water filled syringe was fixed to the banisters of a stairwell and the droplet was dropped onto the particulate bed below. The droplet volume was ~ 10 µl and the impact velocity using this setup were ~7 $m.s^{-1}$, which are comparable to the terminal velocity of a water droplet of 0.27 cm diameter in stagnant air which is 7.7 $m.s^{-1}$ (Gunn & Kinzer, 1949).

The droplet impacts were recorded using a Hotshot 512SC high speed camera (NAC Image Technology, Birmingham, UK); the sample was back lit using a 30 W warm-white LED floodlight. High-speed videos were recorded at 4000 frames per second unless otherwise stated) using a 105 mm F2.8 EX DG Macro lens Sigma, Welwyn Garden City, UK). An external trigger button was used to record the high-speed video just after a single droplet had been released from the needle. The data were processed using HotShot HSSC Link v1.1 software (NAC Image Technology).

Results and discussion

Water droplet impact transitions

Impacts of individual water droplets on hydrophobic surfaces at low velocities allow identification of three distinct regimes of droplet behaviour (Figure 1): droplet rebound, droplet pinning and droplet fragmentation (Reyssat et al. 2006; Tsai et al. 2009). The droplet rebound regime occurs at droplet impact velocities below a critical value (v_{min}, Figure 1a i). At velocities above this ($v > v_{min}$) the droplet becomes pinned to the surface (Figure 1a ii). At higher impact velocities ($v > v^*$) droplet fragmentation occurs and the critical velocity for the onset of such droplet behaviour is defined here as v^* (Figure 1b).

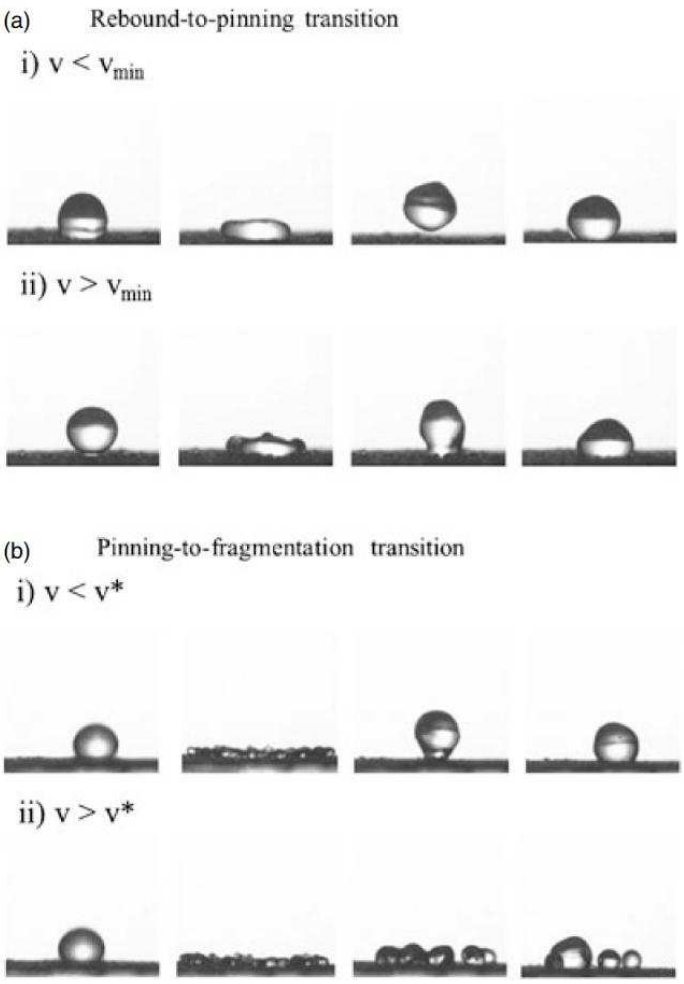

Figure 1 High speed camera images of droplet impact behaviour at (a) vmin and (b) v* transition velocities.

Influence of hydrophobicity

In order to investigate the effect of particulate hydrophobicity on splash behaviour, glass spheres, rendered hydrophilic, were used to form fixed arrays on glass microscope slides; half of these arrays were hydrophobic. Glass microscope slides treated in the same manner as the arrays of glass spheres confirmed the hydrophilic and hydrophobic states by displaying static water contact angles (θ) of about 0 and 117.0^o, respectively.

The hydrophobic particulate surfaces exhibited the three distinct droplet impact regimes with rebound behaviour (Figure 2a i) at the smallest impact velocity studied (~0.3 $m.s^{-1}$) and fragmentation (Figure 2a ii) at impact velocities of ~2.1 $m.s^{-1}$. However, droplet impacts within the range of ~0.3 - ~2.1 $m.s^{-1}$ exhibited solely pinning behavior (Figure 2b). This observation shows the importance of the chemical nature of the particulate surface upon the impact behavior of water droplets.

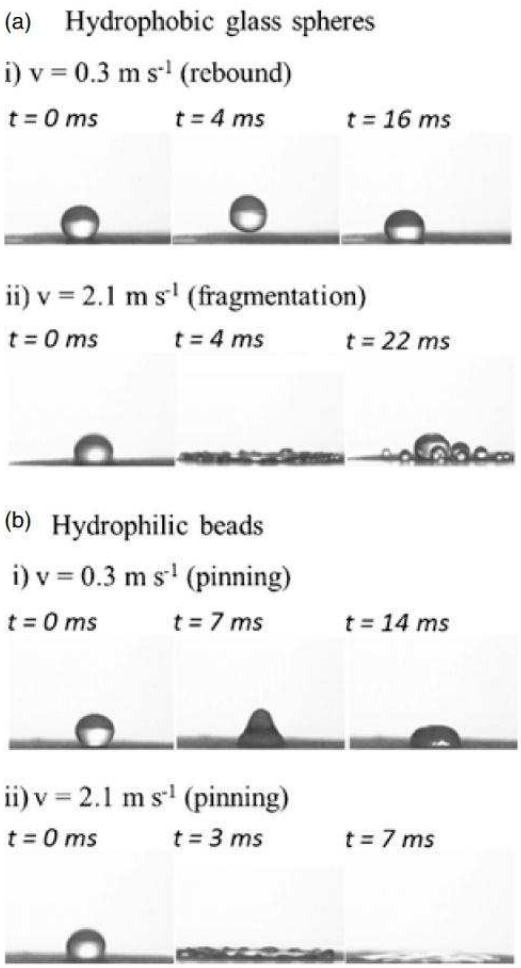

Figure 2 Water droplet impact behaviour on (a) hydrophobic and (b) hydrophilic fixed glass spheres (32–45-μm sieve range).

Although they exhibit solely pinning behaviour on impact with fixed, hydrophilic glass spheres (Figure 2b), the shape and spread of the splash behaviour changed as the impact velocity increased Figure 2b). At an impact velocity of around 0.3 m s^{-1} the profile during impact was of a thicker droplet with a smaller liquid-solid interfacial area (Figure 2b(i)) than that at an impact velocity of about 2.1 m s^{-1}. This observation is consistent with the findings of Roux & Cooper-White (2004), who reported that the thickness of the splash made by an impacting water droplet decreases and the solid-liquid interfacial area increases in order to dissipate the increased kinetic energy as the impact velocity increases.

Influence of particle and droplet size

The diameter of the spheres that made up the fixed, hydrophobic samples influenced the droplet impact behaviour on the arrays. The critical velocity for the rebound-to-pinning transition (v_{min}) was dependent on both particle and droplet size (Figure 3), with v_{min} increasing as the particle size increased (Figure 4). However, the standard error bars show significant overlap, which may result from defects in the particle packing. Rebound behaviour occurs when the gaps between particles are not completely filled by the impacting droplet, which is momentarily in a Cassie-Baxter state (Cassie & Baxter, 1944), as depicted by Figure 5(a). This state allows air pockets to remain within the gaps between surface features, allowing the droplet to completely rebound from the surface upon recoil (Reyssat et al., 2006). At velocities greater than v_{min} the pressure exerted by the impact in the shock envelope (Field, 1999) is enough to force liquid to fill and wet the inside of the gaps between the particles completely, forming a Wenzel state (Wenzel, 1936), as depicted in Figure 5(b). It is the transition between Cassie-Baxter and Wenzel states that occurs at the rebound-to-pinning transition velocity (Lee et al., 2010). In our system, as the diameter of the hydrophobic glass spheres increased, the depth of the gaps between features increased. Therefore, liquid must penetrate further into the gaps in order to achieve the Wenzel state needed for pinning.

Previous work on 'ideal' super-hydrophobic surfaces (Reyssat et al., 2006) suggests a stronger dependence of v_{min} on feature size than we have observed. However, our system differs from the 'model' super-hydrophobic systems described in the literature (Reyssat et al., 2006; Tsai et al., 2009), which tend to employ straight-sided, photo-lithographically defined pillar features. The particles that we have investigated are of similar size to the largest features studied by Reyssat et al. (2006) and also have a curved profile, in contrast to the simpler, straight-sided features of most 'model' super-hydrophobic surfaces. The curved profile of the glass spheres results in a non-uniform distance that the wetting front must bridge as the wetting front advances through the pore. This distance decreases until it reaches a minimum at the throat of the pore, where greater pressure will be required to force the wetting front through the throat of the pore than to pass the top of the feature. This results in vmin having a stronger dependence on feature size for straight-edged features as, in theory, there will be a single threshold penetration pressure required for the transition from a rebound to a pinning state.

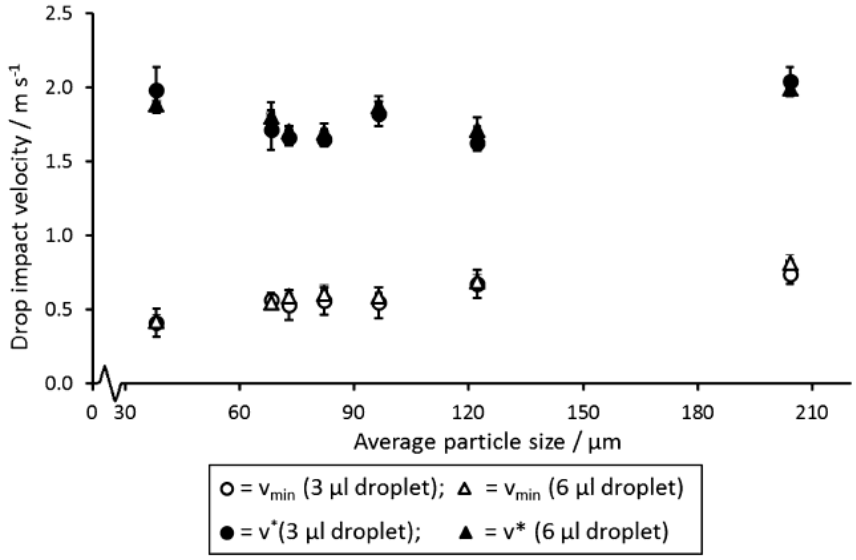

Figure 3 Graph showing v_{min} and v* of two drop sizes on fixed, hydrophobic glass spheres of different sizes (error bars show standard deviation).

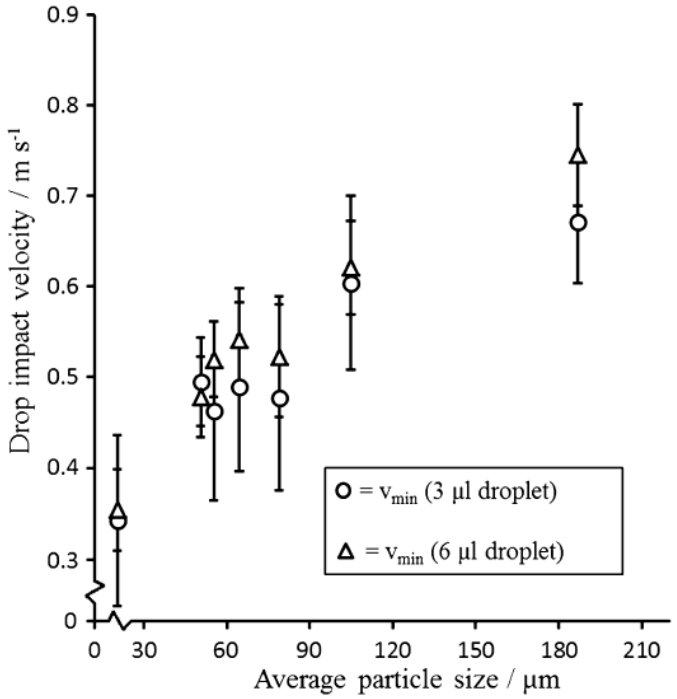

Figure 4 Graph showing v_{min} of two drop sizes on fixed, hydrophobic glass spheres of different sizes (error bars show standard deviation).

Fragmentation behaviour occurs due to the liquid 'pancake' of the impacting droplet breaking up as a result of shock waves at high impact velocities due to either jetting from trapped air in surface features due to asperities 'ripping' the thin liquid layer (Rioboo et al., 2008). We observed that the critical velocity for droplet fragmentation (v*) exhibited no significant dependency on particle size, which is in agreement with previous work (Reysatt et al., 2006).

Table 1 shows the static, advancing and receding contact angles of the various particle sizes of the fixed, hydrophobic particle beds. The advancing contact angle (θ_A) appears to be independent of the

particle size of the fixed, hydrophobic bed. Surprisingly though, the receding contact angle (θ_R), the relevant angle relating to the retraction of the droplet following its expansion upon impact, does not seem to correlate with the rebound-to-pinning transition (v_{min}). This, however, may be due to the large errors of the receding contact angle, possibly due to imperfections in the packing of the particles, masking any correlation of θ_R and v_{min}.

The size of the water droplet appears to have an effect on the impact behaviour. Figure 4 suggests that the smaller droplet (~ 3 µl, depicted by the open triangles in Figure 4) exhibits greater rebound-to-pinning transition velocity (v_{min}) than a larger droplet (~ 6 µl, depicted by the open circles in Figure 4) following impact on a textured surface of the same fixed particle size. However, the errors are too large to for any firm conclusions to be drawn regarding the effect of droplet volume on the impact behaviour.

Influence of particle shape

Fixed layers of hydrophobic sand and glass spheres were studied in order to investigate how the particle shape influences the droplet impact behaviour. The roughness of the sand grains in comparison to the glass spheres is evident in Figure 6 and this appears to influence the impact behaviour of individual water droplets. Water droplets displayed lower transition velocities when colliding with fixed, hydrophobic sand particles (v_{min} = 0.5 m.s^{-1}; v* = 0.7 ± 0.1 m.s^{-1}) than upon impact on fixed, hydrophobic glass spheres (v_{min} = 0.8 ± 0.1 m.s^{-1}; v* = 2.0 ± 0.1 m.s^{-1}) (Figures 5b and 5c). This observed decrease of transition velocities may be due to the sharper, rough topography of sand particles being more likely to pierce the flattened, expanded droplet (second image in both Figure 6b and c) compared with the smooth glass spheres. This is in agreement with the presence of asperities influencing droplet fragmentation as previously reported (Rioboo et al., 2008).

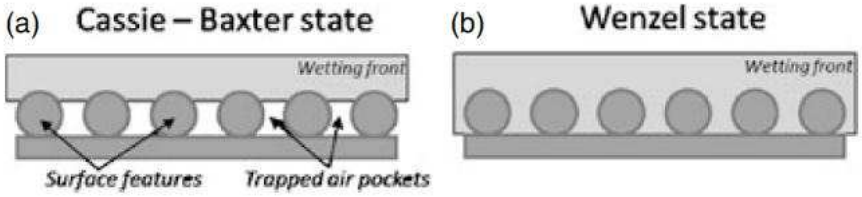

Figure 5 A cartoon representation of the wetting front of a water droplet sitting on a textured surface in the (a) Cassie-Baxter and (b) Wenzel state.

In the case of fixed, hydrophilic particles, the sharp, rough shape of the sand particles appeared to induce droplet fragmentation, though no droplet rebound, upon impact with fixed hydrophilic sand beds (v*= 1.8±0.1 m s^{-1}), whilst the hydrophilic, fixed glass spheres did not exhibit pinning-to-droplet fragmentation over the range of drop impact velocities studied..

Loose particles

Although fixed beds of particles provide a rigid structure for comparison with previous work on superhydrophobic surfaces (Reysatt et al., 2006; Tsai et al., 2009; Lee & Lee, 2011) a more realistic comparison to soils is to study loose particles that are not fixed to a glass microscope slide. Droplet

impacts on loose, particles appears to result in an increase of the rebound-to-pinning transition velocity (v_{min}) with loose, hydrophobic glass spheres of 32-45 µm sieve size exhibiting a higher v_{min} (= 1.5 ± 0.1 $m.s^{-1}$) compared with the fixed analogue (v_{min} = 0.4 ± 0.1 $m.s^{-1}$). This increase may be attributed to the droplet expending less energy recoiling on a loose surface than a fixed one due to the loose surface being able to deform in response to the impact of a droplet. The pinning-to-fragmentation transition seemed unaffected by whether or not the glass spheres were fixed (v* = 2.0 ± 0.2 $m.s^{-1}$ for fixed 32-45 µm hydrophobic glass spheres) or loose (v* = 2.0 ± 0.6 $m.s^{-1}$ for loose, 32-45 µm hydrophobic glass spheres). This observation suggests that the velocities at which v* occurs results in a shock envelope (Field, 1999) that is too high for the particles to absorb via the rearrangement of mobile particles. Such forces cause droplet fragmentation regardless of whether or not the particles are mobile (Rioboo et al., 2008).

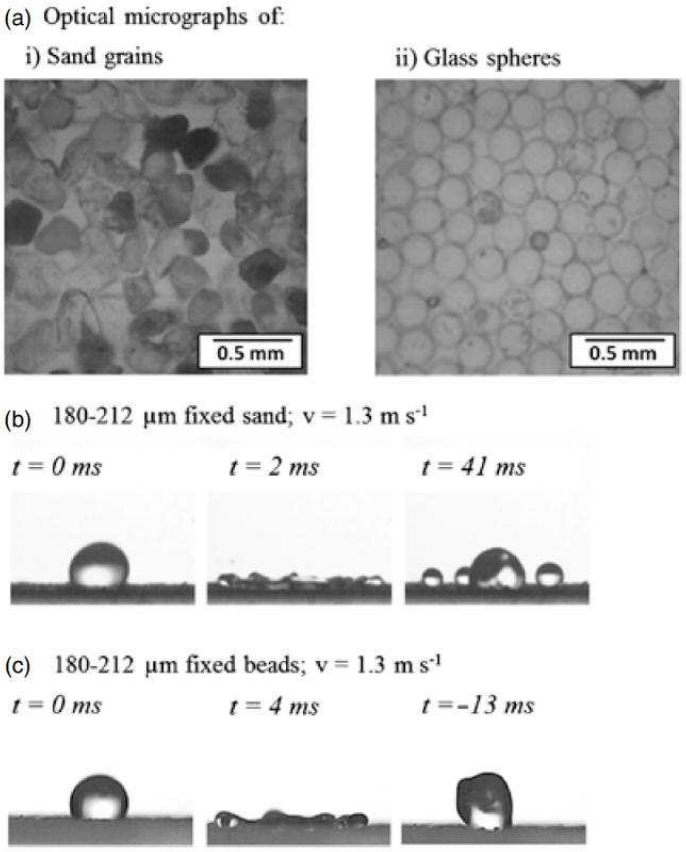

Figure 6 (a) Micrographs of fixed, hydrophobic sand and glass spheres and (b & c) images of drop impacts on fixed, hydrophobic sand and glass, respectively.

High speed camera images of single water droplet impacts on loose, hydrophilic glass spheres (Figure 7a) shows that upon impact the water droplet displaces some of the loose beads before imbibing into the loose particulate bed in less than 0.2 ms. However, water droplets impacting on loose, hydrophobic glass spheres behave in a much different manner (Figure 7b). Upon impact with the loose hydrophobic glass spheres the water droplet not only causes some loose particles to be ejected from the

impact zone (Figure 7b ii) but the recoiling droplet becomes coated with glass spheres (Figure 7b iii and 6b iv). The loose hydrophobic particles coat the impacting droplet due to the presence of an intrinsic water contact angle (i.e. the Young's law one determined by the surface chemistry for water on a single glass particle) favouring attachment of particles, even hydrophobic ones, to the liquid-air interface and the individual particle not being bound to the surface (Figure 7b iii) forming a liquid droplet covered by hydrophobic particles (Figure 7b iv and v). Such particle-coated droplets are known as liquid marbles and they can freely roll around on the particle bed (Aussillous & Quéré, 2001; McEleney et al., 2009; McHale & Newton, 2011). Such liquid marble formation does not occur upon water droplet impact on loose hydrophilic glass spheres (Figure 7a). Therefore, the formation of highly mobile liquid marbles upon droplet impact on loose, hydrophobic particles represents a mode of particle transport that does not occur with hydrophilic particles and this observation may help to explain increased erosion rates of water repellent soil.

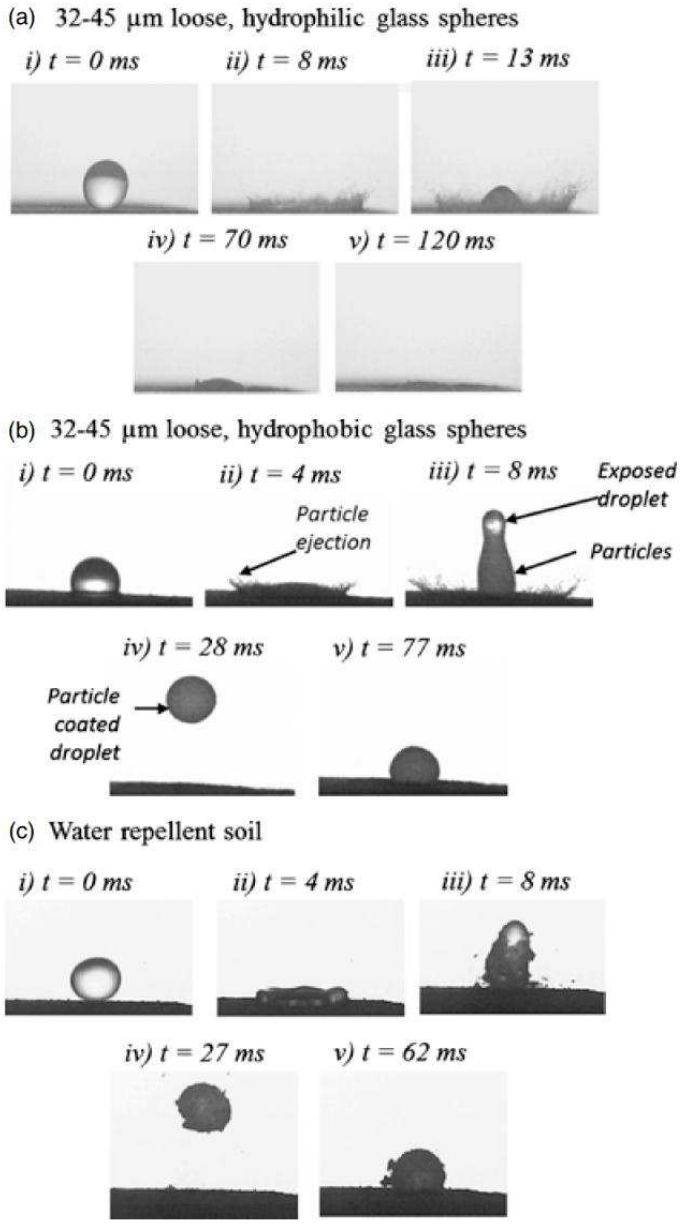

Figure 7 High-speed images of water drop impact on (a) hydrophilic glass spheres, (b) hydrophobic glass spheres and (c) a naturally water repellent soil. All video sequences are of a droplet impact velocity of about 0.9 m s^{-1}.

The impact behaviour of individual droplet impact on naturally very strongly water repellent Portuguese soil was studied and displayed similar transition velocities (v_{min} = 1.4 ± 0.4 $m.s^{-1}$; v* = 1.8 ± 0.7 $m.s^{-1}$) to that of 32-45 μm hydrophobic glass spheres (v_{min} = 1.5 ± 0.1 $m.s^{-1}$; v* = 1.7 ± 0.1 $m.s^{-1}$). Figure 7c shows that the water repellent soil can form liquid marbles in a similar mechanism to glass spheres (Figure 7b). The formation of liquid marbles occurs during fragmentation at the low impact velocities studied.

Droplet impact behaviour at greater velocity

In order to observe more realistic droplet impact behaviour, relative to a rainfall event, high impact velocity tests were carried out on loose hydrophilic and hydrophobic glass spheres and the water repellent Portuguese soil (Figure 8). The impact velocity of the water droplet was ~ 7 ms^{-1}, which is comparable to the terminal velocity of raindrops of ~2.3 mm in diameter in stagnant air (Gunn and Kinzer, 1949).

The 7 m s−1 impact behaviours of single water droplets on loose hydrophilic and hydrophobic glass spheres (Figure 8a,b), first glance, appear to be similar. One apparent similarity of the droplet impacts is that both seem to yield liquid marbles Figure 8a(iii) and b(iii)). However, those in the hydrophilic case were not mobile, unlike those in the hydrophobic case, and were probably more encased by the fragmenting droplet than the hydrophobic beads, which were entrained on the droplet, forming true liquid marble. The mobility of liquid marbles formed by the droplet impact on the loose, hydrophobic glass spheres is evident by the observation of a dry crater remaining after the droplet impact (Figure 8b(vi)). This was caused by the mobile liquid marbles sliding over the surrounding particles, leaving only a small liquid marble trapped in the impact crater. The immobility of the 'liquid marbles' formed by droplet impact on hydrophilic particles is shown by the wet, 'crusty' crater formed at the impact site (Figure 8a(vi)), which results from the liquid droplet fragments being absorbed by the hydrophilic glass particle bed, leaving the encapsulated particles behind (Katsuragi, 2011).

Droplet impact behaviour (at 7 m s^{-1}) on the water-repellent Portuguese soil (Figure 8c) appears to be very similar to on hydrophobic glass spheres as it results in liquid marble formation and leaves a very similar dry impact zone after the droplet impact event. The observation that liquid marbles form during droplet impact on hydrophobic particles (Figures 7, 8b,c) and soil, but not upon droplet impact with hydrophilic particles (Figure 7b), is highly significant and may help to explain enhanced soil erosion rates that have been observed for water-repellent soil conditions (Doerr et al., 2000). The mobility of a liquid marble may present a soil transport mechanism that appears accessible to hydrophobic but not to hydrophilic particulate systems. However, further study of droplet impact behaviour on non-water-repellent soil would be required to confirm whether or not this is the case.

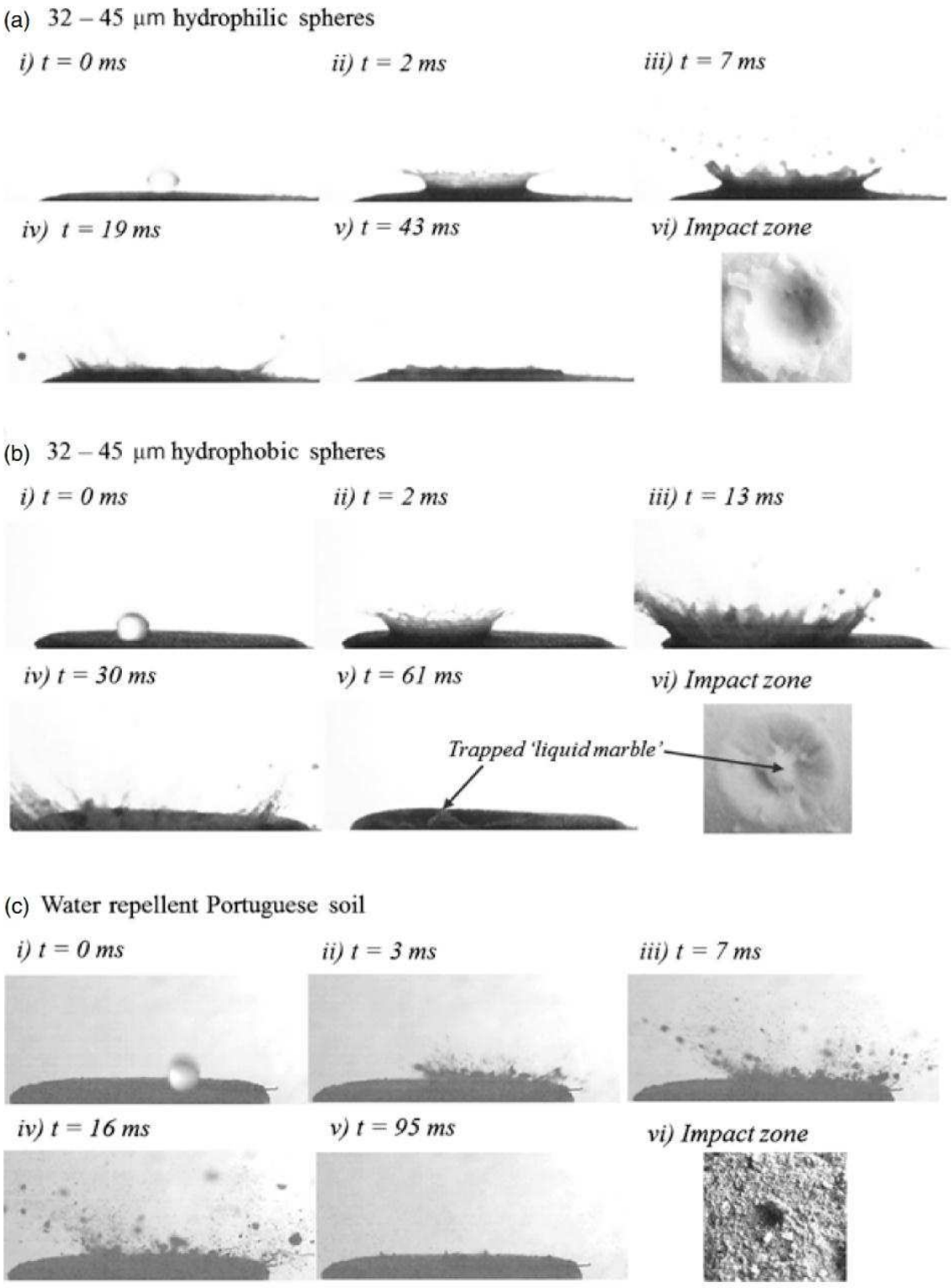

Figure 8 High speed images (recorded at 5000 fps) and photograph of the impact zone of high impact velocity (v=about 7 m s^{-1}) water droplet impacts on (a) hydrophilic glass spheres, (b) hydrophobic glass spheres and (c) a naturally water-repellent soil.

Conclusions

The aim of this study was to investigate water droplet I pact behaviour on water-repellent and wettable particulate matter and to determine whether or not water-repellent glass particles can provide a good model for naturally-occurring highly water repellent soil.

The results show that:

1. The hydrophobicity of the glass spheres is critical to the water droplet displaying the three regimes of impact behaviour.

2. The behaviour of water droplets upon impact with fixed hydrophobic glass spheres is dependent on size of the particles themselves.

3. Particle shape, of fixed hydrophobic surfaces, is also an important factor affecting the initial behaviour of the droplet on striking the surface. Rough, angular particles (such as sand) lead to droplet fragmentation with slower impact velocities than those on smooth particulate surfaces such as glass spheres. However, droplet impact on loose sand grains was not addressed in this study; therefore the increased propensity for droplet fragmentation upon impact with rough particles may not be observed if the impact occurs on loose, rough particles caused by surface reconstruction, providing a means of energy dissipation.

4. The cohesion of the particle bed (whether fixed or loose) affects droplet behaviour. This leads to a greater tendency of the water droplet to rebound from the extremely water-repellent surface and to gather hydrophobic particles on its surface as it does so, leading to the formation of highly mobile liquid marbles.

5. Naturally strongly water-repellent soil behaves in a strikingly similar manner to beds of extremely water-repellent loose hydrophobic glass spheres, where the impact of an individual water droplet forms a coherent liquid marble capable of independent motion. This suggests that factors influencing drop impacts on model particles may provide a reasonable model for the response of water-repellent soil to such impacts.

6. The formation of mobile liquid marbles, at droplet impact velocities approaching that of rainfall, could be a possible mechanism for increased soil erosion of water-repellent soils as the formation of mobile liquid marbles was not observed upon droplet impact on loose, hydrophilic particulate systems.

We have demonstrated that chemically modified glass beads with a single level of water-repellency have been shown to behave in a similar manner to soil of comparable hydrophobicity. Further work will study particulate systems with layers of varying degrees of water-repellency to investigate the importance that the degree of water repellency of sub-surface particulate layers has for droplet impact behaviour.

Supporting Information

The following supporting information is available in the online version of this article:

Table S1. Imbibition times measured during five repeated MED tests of loose Portuguese soil.

Table S2. Imbibition times measured during five repeated MED tests of loose, hydrophobic sand (180–212-μm sieve size).

Table S3. Imbibition times measured during five repeated MED tests of loose, hydrophobic glass particles (180–212-μm sieve size).

Table S4. Imbibition times measured during five repeated MED tests of loose, hydrophobic glass particles (32–45-μm sieve size).

Figure S1. (a) Photograph of the high speed camera set-up and (b) a close-up photograph of the needle and sample.

Figure S2. Drop impact velocity versus drop height for 3 and 6 μl droplets. The equations of the curves fitted to the data are also shown and used to convert the transitional droplet heights (h_{min} and h*) to transitional droplet velocities (v_{min} and v*).

Acknowledgements

We thank the UK Engineering and Physical Sciences Research Council (EPSRC) for funding under grants EP/H000704/1, EP/H000747/1 and EP/E063489/1.

References

Atanassova, A. & Doerr, S.H., 2010. Organic compounds of different extractability in total solvent extracts from soils of contrasting water repellency. European Journal of Soil Science, **61**, 298-313.

Aussillous P., Quéré D. 2001. Liquid marbles. Nature, **411**, 924–927.

Bachmann, J. & McHale, G. 2009. Superhydrophobic surface: A model approach to predict contact angle and surface energy of soil particles. European Journal of Soil Science, **60**, 420-430.

Beard, K.V. 1976. Terminal velocity and shape of cloud and precipitation drops aloft. Journal of the Atmospheric Sciences, **33**, 851-864.

Bisdom, E.B.A., Dekker, L.W. & Schoute, J.F.Th. 1993. Water repellency of sieve fractions from sandy soils and relationships with organic material and soil structure. Geoderma, **56**, 105-118.

Cassie, A.B.D. & Baxter, S. 1944. Wettability of porous surfaces. Transactions of the Faraday Society, **40**, 546-551.

DeBano, L.F. 2000. Water repellency in soils: A historical overview. Journal of Hydrology, **231-232**, 4-32.

Dekker, L.W. & Ritsema, C.J. 1994. How water moves in a water repellent sandy soil 1. Potential and actual water repellency. Water Resources Research, **30**, 2507-2517.

Dekker L.W., Doerr, S.H., Oostindie, K., Ziogas, A.K., & Ritsema, C.J. 2001. Water repellency and critical soil water content in a dune sand. Soil Science Society of America Journal, **65**, 1667-1674.

Doerr, S.H. 1998. On standardizing the 'water drop penetration time' and the 'molarity of an ethanol droplet' techniques to classify soil hydrophobicity: A case study using medium term textured soils. Earth Surface Processes and Landforms, **23**, 663-668.

Doerr S.H., R.A. Shakesby, R.A., & Walsh, R.P.D. 2000. Soil water repellency, its characteristics, causes and hydro-geomorphological consequences. Earth Science Reviews, **51**, 33-65.

Doerr, S.H., Shakesby, R.A., Dekker, L.W., & Ritsema, C.J. 2006. Occurrence, prediction and hydrological effects of water repellency amongst major soil and land use types in a humid temperate climate. European Journal of Soil Science, **57**, 741–754.

Ellerbrock, R.H, Gerke H.H., Bachmann, J. and Goebel, M.-O. 2005. Composition of organic matter fractions for explaining wettability of three forest soils. Soil Science Society of America Journal, **69,** 57-66.

Field, J.E. 1999. Liquid impact, theory, experiment, applications. Wear, **233-235**, 1-12.

Gunn, R and Kinzer, G.D. 1949. The terminal velocity of fall for water droplets in stagnant air. Journal of Meteorology, **6**, 243-248.

Hallett, P.D., Nunan, N., Douglas, J.T. & Young, I.M. 2004. Millimeter-scale variability in soil water sorptivity: scale, surface elevation and subcritical repellency effects. Soil Science Society of America Journal, **68**, 352-358.

Hamlett, C.A.E., Shirtcliffe, N.J., McHale, G., Ahn, S., Bryant, R., Doerr, S.H. et al. 2011. Effect of particle size on droplet infiltration into hydrophobic porous media as a model of water repellent soil. Environmental Science & Technology, **45**,

Katsuragi, H. 2011. Length and time scales of a liquid drop impact and penetration into a granular layer. The Journal of Fluid Mechanics, **675**, 552-573.

Kwon, H.M., Paxson, A.T., Varanasi, K.K. and Patankar, N.A. 2011. Rapid deceleration-driven wetting transition during pendant drop deposition on superhydrophobic surfaces. Physical Review Letters, **106**, 036102.

Lee, J.B & Lee, S.H. 2011. Dynamic wetting and spreading charateristics of a liquid droplet impinging on hydrophobic textured surfaces. Langmuir, **27**, 6565-6573.

Lee, J.B., Gwon, H.R., Lee, S.H. & Cho, M. 2010. Wetting transition characteristics on microstructured hydrophobic surfaces. Materials Transactions, **51**, 1709–1711.

McEleney, P., Walker, G.M., Larmour, I.A. & Bell, S.E.J. 2009. Liquid marble formation using hydrophobic powders. Chemical Engineering Journal, **147**, 373-382.

McHale, G. & Newton, M.I. 2011. Liquid marbles: principles and applications. Soft Matter, **7**, 3473-3481.

McHale, G., Newton, M. I. & Shirtcliffe, N.J. 2005. Water-repellent soil and its relationship to granularity, surface roughness and hydrophobicity: a materials science view. European Journal of Soil Science, **56**, 445-452.

McHale, G., Shirtcliffe, N.J., Newton, M.I. & Pyatt, F.B. 2007. Implications of ideas on super-hydrophobicity on water repellent soil. Hydrological Processes, **21**, 2229-2238.

Mueller, K. & Deurer M. 2011. Review of the remediation strategies for soil water repellency. Agriculture Ecosystems & Environment, **144**, 208-221.

Reyssat, M., Pépin, Marty, F., Chen, Y. & Quéré, D. 2006. Bouncing transitions on microtextured materials. Europhysics Letters, **74**, 306-312.

Rioboo, R., Voué, M., Vaillant, A. & De Coninck, J. 2008. Drop impact on porous superhydrophobic polymer surfaces. Langmuir, **24**, 14074-14077.

Roach, P., Shirtcliffe, N.J. & Newton, M.I. 2008. Progress in superhydrophobic surface development. Soft Matter, **4**, 224-240.

Roux, D.C.D. and Cooper-White, J.J. 2004. Dynamics of water spreading on a glass surface. Journal of Colloid and Interface Science, **277**, 424-436.

Shirtcliffe, N.J., McHale, G., Newton, M.I. & Pyatt, F.B. 2006. Critical conditions of the wetting of soils. Applied Physics Letters, **89**, 094101.

Terry, J.P. & Shakesby, R.A. 1993. Soil water repellency effects on rainsplash: simulated rainfall and photographic evidence. Earth Surface Processes and Landforms, **18**, 519–525.

Tsai, P., Pacheco, S., Pirat, C., Lefferts, L. & Lohse, D. 2009. Drop impact upon micro- and nanostructured superhydrophobic surfaces. Langmuir, **25**, 12293-12298.

Wenzel, R. 1936. Resistance of solid surfaces to wetting by water. Industrial and Engineering Chemistry, **28**, 988-994.

Supplementary Material

a) High speed camera setup

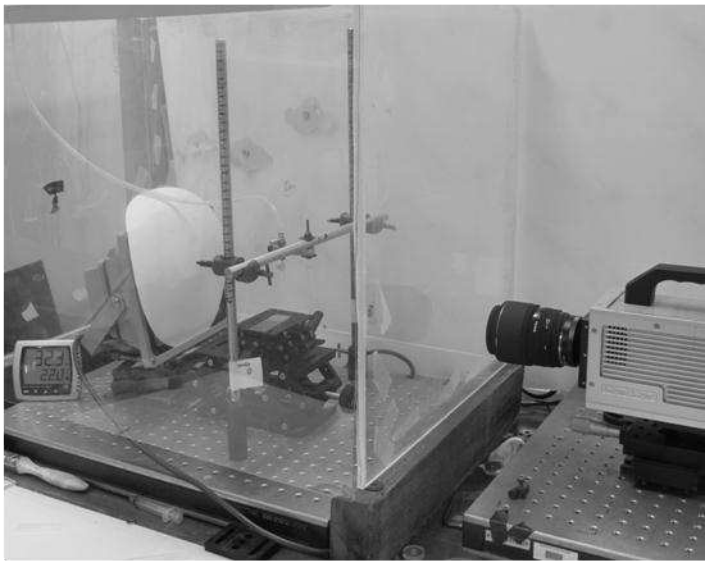

b) The needle and sample

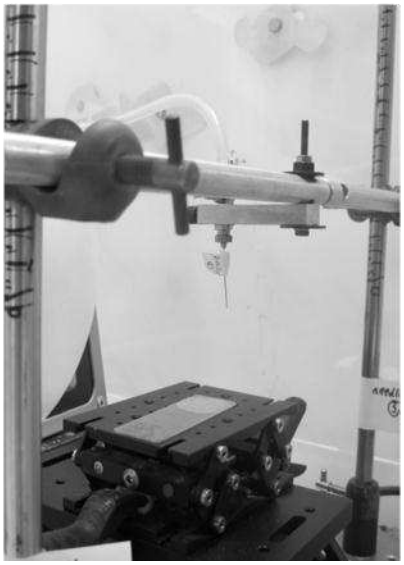

Figure S1 a) Photograph of the high speed camera setup for droplet impact velocities of $\leq$ ~2m.s^{-1} and b) a close up photograph of the needle and sample.

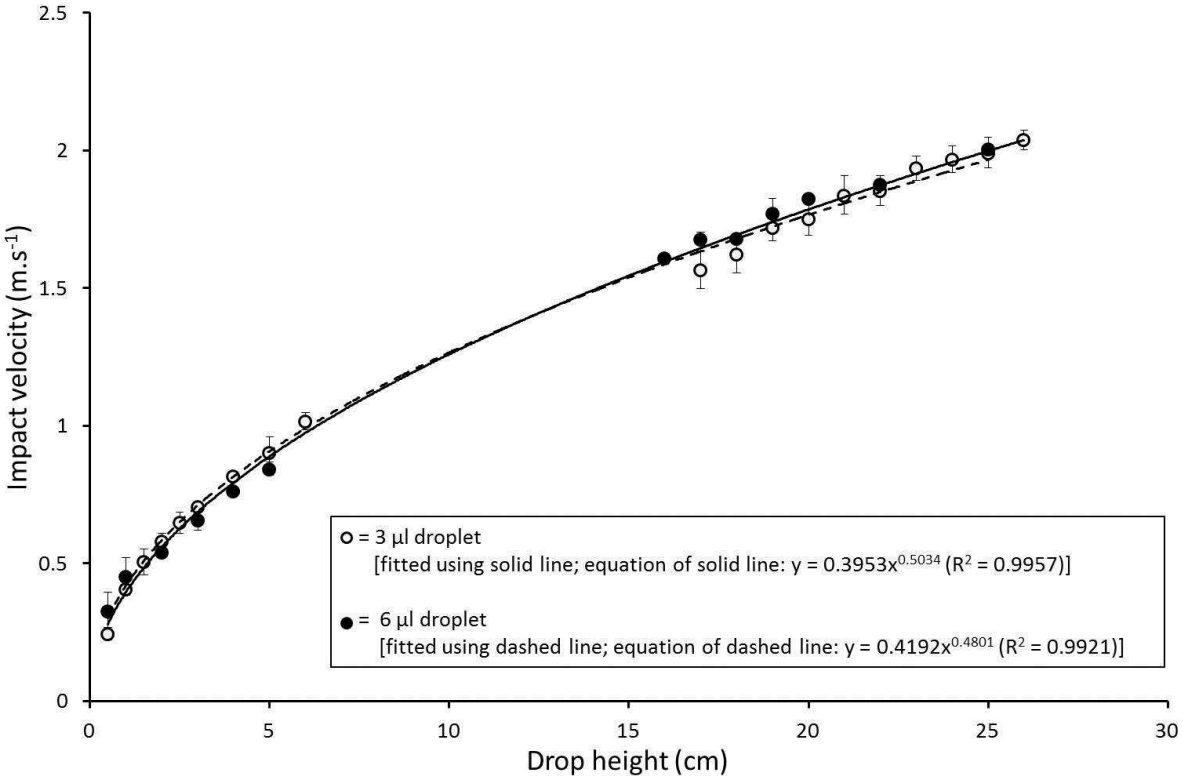

Figure S2 Drop impact velocity vs drop height for 3 µl and 6 µl droplets. The equations of the curves fitted to the data are also shown and used to convert the transitional droplet heights (h_{min} and h*) to transitional droplet velocities (v_{min} and v*).

Table S1 Imbibition times measured during five repeated MED tests of loose Portuguese soil.

Ethanol concentration (vol%)	**Imbibition time (s)**				
	Run 1	Run 2	Run 3	Run 4	Run 5
36	0.81	0.59	0.55	0.4	0.34
24	0.72	0.62	0.75	0.89	0.55
13	7.21	5.40	6.58	4.76	8.54
8.5	>600	>600	>600	>600	>600
3	>600	>600	>600	>600	>600
0	>600	>600	>600	>600	>600

Table S2 Imbibition times measured during five repeated MED tests of loose, hydrophobic sand (180-212 μm sieve size)

Ethanol concentration (%)	**Imbibition time (s)**				
	Run 1	Run 2	Run 3	Run 4	Run 5
36	>600	>600	>600	>600	>600
24	>600	>600	>600	>600	>600
13	>600	>600	>600	>600	>600
8.5	>600	>600	>600	>600	>600
3	>600	>600	>600	>600	>600
0	>600	>600	>600	>600	>600

Table S3 Imbibition times measured during five repeated MED tests of loose, hydrophobic glass spheres (180-212 μm sieve size)

Ethanol concentration (%)	**Imbibition time (s)**				
	Run 1	Run 2	Run 3	Run 4	Run 5
36	2.14	1.78	2.03	1.62	1.47
24	>600	>600	>600	>600	>600
13	>600	>600	>600	>600	>600
8.5	>600	>600	>600	>600	>600
3	>600	>600	>600	>600	>600
0	>600	>600	>600	>600	>600

Table S4 Imbibition times measured during five repeated MED tests of loose, hydrophobic glass spheres (32-45 μm sieve size)

Ethanol concentration (%)	**Imbibition time (s)**				
	Run 1	Run 2	Run 3	Run 4	Run 5
36	>600	>600	>600	>600	>600
24	>600	>600	>600	>600	>600
13	>600	>600	>600	>600	>600
8.5	>600	>600	>600	>600	>600
3	>600	>600	>600	>600	>600
0	>600	>600	>600	>600	>600